

# Light WIMP search in XMASS

K. Abe<sup>a,c</sup>, K. Hieda<sup>a</sup>, K. Hiraide<sup>a,c</sup>, S. Hirano<sup>a</sup>, Y. Kishimoto<sup>a,c</sup>,  
 K. Kobayashi<sup>a,c</sup>, S. Moriyama<sup>a,c</sup>, K. Nakagawa<sup>a</sup>, M. Nakahata<sup>a,c</sup>,  
 H. Ogawa<sup>a,c</sup>, N. Oka<sup>a</sup>, H. Sekiya<sup>a,c</sup>, A. Shinozaki<sup>a</sup>, Y. Suzuki<sup>a,c</sup>,  
 A. Takeda<sup>a,c</sup>, O. Takachio<sup>a</sup>, K. Ueshima<sup>a,1</sup>, D. Umemoto<sup>a</sup>, M. Yamashita<sup>a,c</sup>,  
 B. S. Yang<sup>a</sup>, S. Tasaka<sup>b</sup>, J. Liu<sup>c</sup>, K. Martens<sup>c</sup>, K. Hosokawa<sup>e</sup>, K. Miuchi<sup>e</sup>,  
 A. Murata<sup>e</sup>, Y. Onishi<sup>e</sup>, Y. Otsuka<sup>e</sup>, Y. Takeuchi<sup>e,c</sup>, Y. H. Kim<sup>f</sup>, K. B. Lee<sup>f</sup>,  
 M. K. Lee<sup>f</sup>, J. S. Lee<sup>f</sup>, Y. Fukuda<sup>g</sup>, Y. Itow<sup>h,d</sup>, K. Masuda<sup>h</sup>, Y. Nishitani<sup>h</sup>,  
 H. Takiya<sup>h</sup>, H. Uchida<sup>h</sup>, N. Y. Kim<sup>i</sup>, Y. D. Kim<sup>i</sup>, F. Kusaba<sup>j</sup>, D. Motoki<sup>k,1</sup>,  
 K. Nishijima<sup>j</sup>, K. Fujii<sup>l</sup>, I. Murayama<sup>l</sup>, S. Nakamura<sup>l</sup>

<sup>a</sup>*Kamioka Observatory, Institute for Cosmic Ray Research, the University of Tokyo,  
 Higashi-Mozumi, Kamioka, Hida, Gifu, 506-1205, Japan*

<sup>b</sup>*Information and multimedia center, Gifu University, Gifu 501-1193, Japan*

<sup>c</sup>*Kavli Institute for the Physics and Mathematics of the Universe, the University of  
 Tokyo, Kashiwa, Chiba, 277-8582, Japan*

<sup>d</sup>*Kobayashi-Maskawa Institute for the Origin of Particles and the Universe, Nagoya  
 University, Furo-cho, Chikusa-ku, Nagoya, Aichi, 464-8602, Japan.*

<sup>e</sup>*Department of Physics, Kobe University, Kobe, Hyogo 657-8501, Japan*

<sup>f</sup>*Korea Research Institute of Standards and Science, Daejeon 305-340, South Korea*

<sup>g</sup>*Department of Physics, Miyagi University of Education, Sendai, Miyagi 980-0845,  
 Japan*

<sup>h</sup>*Solar Terrestrial Environment Laboratory, Nagoya University, Nagoya, Aichi 464-8602,  
 Japan*

<sup>i</sup>*Department of Physics, Sejong University, Seoul 143-747, South Korea*

<sup>j</sup>*Department of Physics, Tokai University, Hiratsuka, Kanagawa 259-1292, Japan*

<sup>k</sup>*School of Science and Technology, Tokai University, Hiratsuka, Kanagawa 259-1292,  
 Japan*

<sup>l</sup>*Department of Physics, Faculty of Engineering, Yokohama National University,  
 Yokohama, Kanagawa 240-8501, Japan*

---

## Abstract

A search for light dark matter using low-threshold data from the single phase liquid xenon scintillation detector XMASS, has been conducted. Using

---

<sup>1</sup>Now at Research Center for Neutrino Science, Tohoku University, Sendai 980-8578, Japan

the entire 835 kg inner volume as target, the analysis threshold can be lowered to 0.3 keVee (electron-equivalent) to search for light dark matter. With low-threshold data corresponding to a 5591.4 kg·day exposure of the detector and without discriminating between nuclear-recoil and electronic events, XMASS excludes part of the parameter space favored by other experiments.

*Keywords:* Dark Matter, WIMP, xenon

---

## 1. Introduction

There is substantial evidence that the universe is composed of dark matter [1]. Among the most plausible dark matter candidates, Weakly Interacting Massive Particles (WIMPs), which are expected to couple to ordinary matter primarily through the weak force, can be detected directly through observation of nuclear recoils produced in their elastic scattering interactions with detector nuclei [2]. Many theories of physics beyond the Standard Model predict stable WIMPs with supersymmetric models still among the most popular [3]. In the constrained Minimal Supersymmetric Standard Model, the lightest supersymmetric particle is favored as a WIMP candidate and has an expected mass of  $M_\chi > 100$  GeV. However, some experiments indicate a possible WIMP signal [4, 5, 6] with a lighter mass of  $\sim 10$  GeV and with a spin-independent cross section of the order of  $\sim 10^{-40}$  cm<sup>2</sup>. These positive signals have come predominantly from experiments without the capability to discriminate between electromagnetic and nuclear recoils, while other experiments that have this ability have excluded light WIMPs at these cross sections [7, 8, 9]. This Letter presents a search for light WIMPs using a 5591.4 kg·day exposure of the XMASS experiment without nuclear recoil discrimination.

## 2. XMASS detector

The XMASS experiment is located underground in the Kamioka Observatory at a depth of 2700 m.w.e. and has been designed to search for WIMP interactions using the self-shielding properties of liquid xenon in an ultra low radioactivity environment [10]. XMASS is a single phase liquid xenon scintillator detector containing 1050 kg of Xe in an OFHC copper vessel. Xenon scintillation light is collected by 630 hexagonal and 12 cylindrical inward-pointing Hamamatsu R10789 series photomultiplier tubes (PMTs) arranged

on an 80 cm diameter pentakis-dodecahedron support structure within the vessel to give a total photocathode coverage of 62.4 %.

These PMTs view an active target region containing 835 kg of liquid xenon. In order to monitor the PMT stability and measure the trigger efficiency, eight blue LEDs with Teflon diffusers are mounted to the support structure. There are six LEDs arranged along the equator and one each at the top and the bottom of the pentakis-dodecahedron. To shield the scintillator volume from external gammas, neutrons, and muon-induced backgrounds, the copper vessel is placed at the center of a  $\phi 10\text{ m} \times 11\text{ m}$  cylindrical tank filled with pure water. This volume is viewed by 72 Hamamatsu R3600 20-inch PMTs to provide both an active muon veto and passive shielding against these backgrounds. This is the first water Cherenkov shield used in a dark matter search experiment. To perform energy and position reconstruction calibrations a portal has been prepared along the central vertical axis ( $z$ -axis) of the PMT support structure through which an OFHC copper rod can be inserted directly into the target volume. Thin cylindrical calibration sources containing either of  $^{55}\text{Fe}$ ,  $^{57}\text{Co}$ ,  $^{109}\text{Cd}$ , or  $^{241}\text{Am}$  are placed at the tip of this rod to perform detector calibrations. A more detailed description of the XMASS detector is presented in [11].

PMT signals are passed through preamplifiers with a voltage gain factor of 11 before being processed by Analog-Timing-Modules (ATMs) [12]. These modules combine the functions of typical ADC and TDC modules, recording both the integrated charge and the arrival time of each PMT signal. For each PMT channel the discriminator threshold is set to  $-5\text{ mV}$ , which corresponds to 0.2 photoelectrons (p.e.). When a PMT signal is above threshold a “hit” is registered on the module. A global trigger is generated based on the number of hit PMTs within a 200 ns window.

A complete XMASS detector Monte Carlo (MC) simulation package based on Geant4 [13] and including readout electronics has been developed [11] and used for this analysis. The simulation has been tuned using calibration data and the optical properties of the liquid xenon have been determined empirically using data taken at nine points along the  $z$ -axis:  $z = \pm 40\text{ cm}$ ,  $\pm 30\text{ cm}$ ,  $\pm 20\text{ cm}$ ,  $\pm 10\text{ cm}$ ,  $0\text{ cm}$ .

### 3. Data and Event Selection

The data used for this analysis, corresponding to 6.70 days of livetime, was taken in February 2012 with a low trigger threshold of four PMT hits.

Using 122 keV gammas from the  $^{57}\text{Co}$  calibration source the xenon light yield was found to be 14.7 photoelectrons/keVee. This large light yield allows the analysis threshold to be lowered sufficiently for sensitivity to low mass WIMPs. In order to achieve optimal sensitivity, the entire detector volume is used because fiducialization is increasingly difficult at these low energies.

In the analysis presented below, the nuclear-recoil equivalent energy ( $E_{\text{NR}}$ ) is determined by conversion from electron equivalent energy ( $E_{\text{ee}}$ ) using the scintillation efficiency,  $\mathcal{L}_{\text{eff}}$ , for nuclear recoils relative to that of 122 keV gammas at zero electric field. The treatment of the energy dependence of  $\mathcal{L}_{\text{eff}}$  and its uncertainty is the same as in Ref. [14]. The resulting functional dependence of  $E_{\text{NR}}$  on  $E_{\text{ee}}$  with its one- $\sigma$  uncertainty is shown in Fig. 1. To illustrate the impact of this uncertainty on the present analysis, the 0.3 keVee analysis threshold is also shown in the figure. In the  $\mathcal{L}_{\text{eff}}$  framework, though the absolute energy scale is determined at 122 keVee, dark matter signals are expected to appear at lower energies. Lower energy calibration samples are used to evaluate the accuracy of the detector simulation at these lower energies. Fig. 2 shows the ratio of the total number of observed photoelectrons relative to the simulation's prediction as a function of the electron equivalent energy for several calibration samples. The apparent deviation of the simulation from the data reflects not only imperfection in the modeling of the detector environment but also the non-linear response of electron-mediated events in liquid xenon [15]. Since the 5.9 keV X-ray from  $^{55}\text{Fe}$  is the lowest energy calibration point, the response at lower energies is extrapolated using a linear fit through all calibration energies. In the analysis the fitting error from this procedure, 1.3% at 0.3 keVee, is treated as a systematic effect on the energy scale. However, the effect of this uncertainty is small relative to that induced by the uncertainty in  $\mathcal{L}_{\text{eff}}$ , which is 13% at the same energy.

The trigger efficiency as a function of the total number of photoelectrons near the trigger threshold is smeared by the response of the electronics. Moreover, the trigger efficiency depends upon the WIMP mass since the distribution of the expected number of hits is a function of that mass. For this reason the trigger efficiency near threshold is derived using LED data taken at single photoelectron level intensities in conjunction with the detector simulation. During the measurement LEDs are flashed at 100 Hz and each flash of the LED is recorded regardless of the number of PMT hits observed. Based on this information the distribution of the number of hit PMTs, the  $n_{\text{hit}}$  distribution, is formed for each LED. Using the detector simulation the same distribution is made for each WIMP mass (The astro-

physical parameters used in this simulation are described in Section 4). Each LED event is then reweighted based on the ratio of the nhit distributions so that the number of expected photoelectrons, and hence energy, for a WIMP signal can be derived from the LED data. Comparison of the number of LED flashes with the number of global triggers issued by the ATMs is then used to compute the expected WIMP trigger efficiency as a function of the observed energy. The resulting efficiency curves for representative masses from the allowed region of [5] are shown in Fig. 3. The analysis threshold is chosen as the energy at which the trigger efficiency is greater than 50 % for 5 GeV WIMPs and corresponds to 0.3 keVee. The error bars in the figure illustrate that the trigger efficiency varies somewhat based upon which LED is used. This variation reflects intrinsic differences in the LEDs themselves as well as a possible position dependence of the detector response and is therefore treated as a systematic error in the analysis. A 1.5% error is determined at 0.3 keVee. Using only the predicted nhit distribution from the WIMP simulation, the efficiency curve's shape is well reproduced within errors.

The energy spectrum for all events in the entire volume of the detector over a 5591.4 kg·day exposure is shown in Fig. 5. To remove backgrounds prior to analysis three types of timing cuts are applied to the raw data. In order to remove events caused by the tail of the scintillation light distribution observed in energetic gamma, beta, alpha, and muon interactions within XMASS, events that occurred within 10 ms of the previous event are rejected. Events whose timing distribution has an RMS greater than 100 ns are also removed. The last and most significant cut is designed to remove events which produce light predominantly through Cherenkov emission, in particular the beta particle emitted in the decay of  $^{40}\text{K}$  contamination in the PMT photocathode. To select these events a time-of-flight correction is made to the timing distribution of each event assuming the event vertex is on the surface of the PMT closest to the charge-weighted center of gravity of the event. After this correction the timing distribution of Cherenkov-like events is found to be narrower than that for scintillation-like events. Events with more than 60 % of their PMT hits occurring within the first 20 ns of the event window are removed as Cherenkov-like. The ratio of the number of PMT hits within the first 20 ns relative to the total number of hits in the event window for all events (head-to-total ratio) is shown in Fig. 4. Each step of the data reduction is shown in Fig. 5.

The expected WIMP acceptance efficiency of these cuts was estimated with the detector simulation. In the simulation WIMP recoil energy spec-

tra were generated for each WIMP mass and MC events were distributed uniformly throughout the detector volume using a liquid scintillation decay constant of 25 ns [16]. Fig. 6 shows the resulting signal acceptance efficiency at energies below 1 keVee. The size of the error bars comes primarily from the systematic uncertainty in the xenon scintillation decay constant,  $25 \pm 1$  ns, which is estimated based on the difference between the XMASS model [16] and the NEST model [17] based on [18]. A systematic error on the selection efficiency is determined based on the error resulting from a linear fit to the points in the figure. At the 0.3 keVee analysis threshold this error is 6.1%.

#### 4. Results and Discussion

Figure 7 shows simulated WIMPs energy spectra overlaid on the observed spectrum after the data reduction was applied. WIMPs are assumed to be distributed in an isothermal halo with  $v_o = 220$  km/s, a galactic escape velocity of  $v_{\text{esc}} = 650$  km/s, and an average density of  $0.3 \text{ GeV/cm}^3$ . In order to set a conservative upper bound on the spin-independent WIMP-nucleon cross section, the cross section is adjusted until the expected event rate in XMASS does not exceed the observed one in any energy bin above 0.3 keVee. Implementing the systematic errors discussed in the text above, the resulting 90% confidence level (C.L.) limit derived from this procedure is shown in Fig. 8. The impact of the uncertainty from  $\mathcal{L}_{\text{eff}}$  is large in this analysis, so its effect on the limit is shown separately in the figure.

After careful study of the events surviving the analysis cuts, their origins are not completely understood. Contamination of  $^{14}\text{C}$  in the GORE-TEX<sup>®</sup> sheets between the PMTs and the support structure may explain a fraction of the events. Light leaks through this material are also suspect. Nonetheless, the possible existence of a WIMP signal hidden under these and other backgrounds cannot be excluded. Although no discrimination has been made between nuclear-recoil and electronic events, and many events remain in the analysis sample, the present result excludes part of the parameter space favored by other measurements [4, 5, 6] when those data are interpreted as a signal for light mass WIMPs. Finally, we are working on modifications to the inner surface of XMASS, especially around the PMTs, to improve the detector performance.

## Acknowledgments

We gratefully acknowledge the cooperation of Kamioka Mining and Smelting Company. This work was supported by the Japanese Ministry of Education, Culture, Sports, Science and Technology, Grant-in-Aid for Scientific Research, and partially by the National Research Foundation of Korea Grant funded by the Korean Government (NRF-2011-220-C00006).

## References

- [1] J. Beringer et al. (Particle Data Group), Phys. Rev. D86, 010001 (2012).
- [2] M. W. Goodman and E. Witten, Phys. Rev. D31, (1985) 2059.
- [3] G.Jungman, M.Kamionkowski, and K.Griest, Phys. Rep. 267 (1996) 195.
- [4] R. Bernabei et al., Eur. Phys. J. C 56, (2008) 333; R. Bernabei et al., Eur. Phys. J. C 67, (2010) 39.
- [5] C. E. Aalseth et al., Phys. Rev. Lett., 106 131301 (2011).
- [6] G.Angloher et al., Eur. Phys. J. C 72 (2012) 1971.
- [7] E. Aprile et al., arXiv:1207.5988; J. Angle et al., Phys. Rev. Lett. 107 051301 (2011).
- [8] Z. Ahmed et al., Science 327, (2010) 1619; Z. Ahmed et al., Phys. Rev. Lett. 106 131302 (2011).
- [9] E. Armengaud et al., Phys. Rev. D 86, 051701(R) (2012)
- [10] Y. Suzuki, arXiv:hep-ph/0008296.
- [11] K. Abe et al., NIM-A, in preparation; arXiv:1301.2815.
- [12] S. Fukuda et al., Super-Kamiokande collaboration, Nucl. Instrum. Meth. A501 (2003) 418.
- [13] S. Agostinelli et al., Nucl. Instr. Meth. A 506 (2003) 250; K. Amako et al., IEEE Trans. Nucl. Sci. 53 (2006).
- [14] E. Aprile et al., Phys. Rev. Lett. 107 131302 (2011).

- [15] E. Aprile et al., arXiv:1209.3658.
- [16] K. Ueshima, Doctor thesis, 2010, University of Tokyo; K. Ueshima et al., Nucl. Instr. and Meth. A 659 (2011) 161.
- [17] M. Szydagis et al., JINST 6 P10002 (2011); NEST (Noble Element Simulation Technique) <http://nest.physics.ucdavis.edu/site/>
- [18] J. V. Dawson et al., Nucl. Instr. and Meth. A 545 (2005) 690.



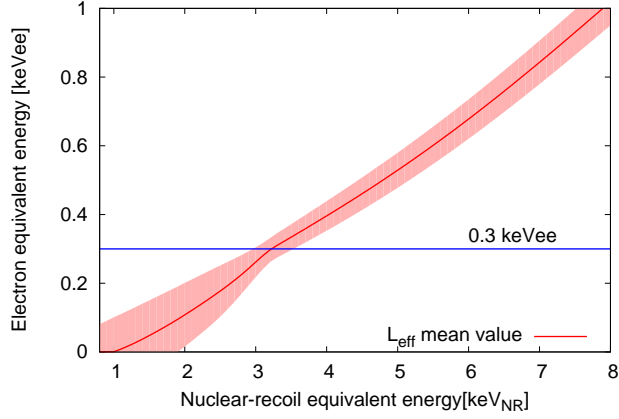


Figure 1: The relationship between the electron equivalent energy and the nuclear-recoil equivalent energy based on the  $\mathcal{L}_{\text{eff}}$  method of Ref. [14]. The one- $\sigma$  uncertainty and the 0.3 keVee analysis threshold are also shown.

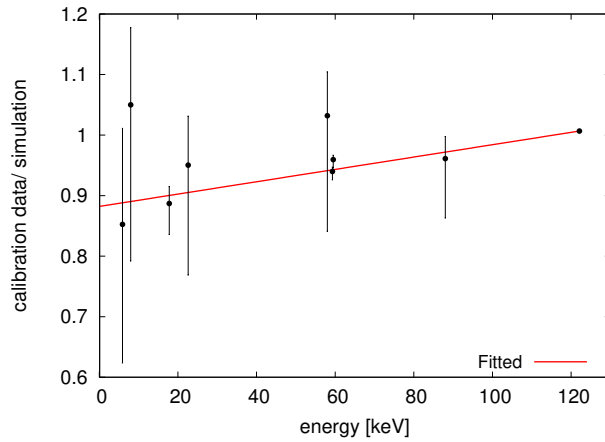


Figure 2: Energy scale comparison between calibration data and simulation results. Calibrations were conducted at 122 keV ( $^{57}\text{Co}$ ), 88 keV, 58 keV, 22 keV, 8 keV ( $^{109}\text{Cd}$ ), 59.5 keV, 17.8 keV ( $^{241}\text{Am}$ ), and 5.9 keV ( $^{55}\text{Fe}$ ). The error bars in the figure stem from uncertainties in the surface reflection properties of the calibration source housing within the simulation.

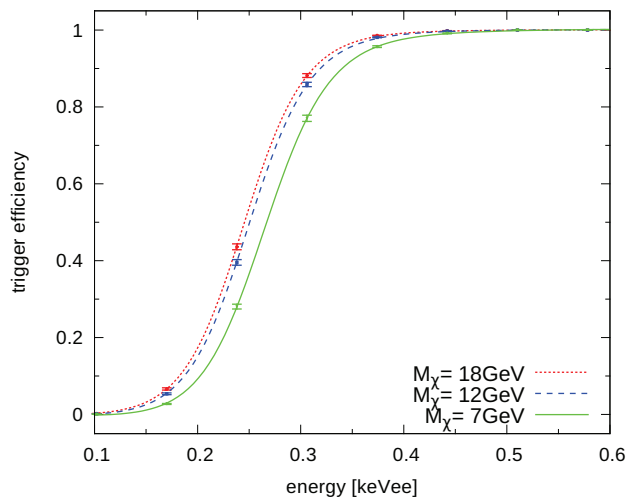


Figure 3: Expected trigger efficiencies for 7 GeV, 12 GeV, and 18 GeV WIMPs derived from LED data in the XMASS detector.

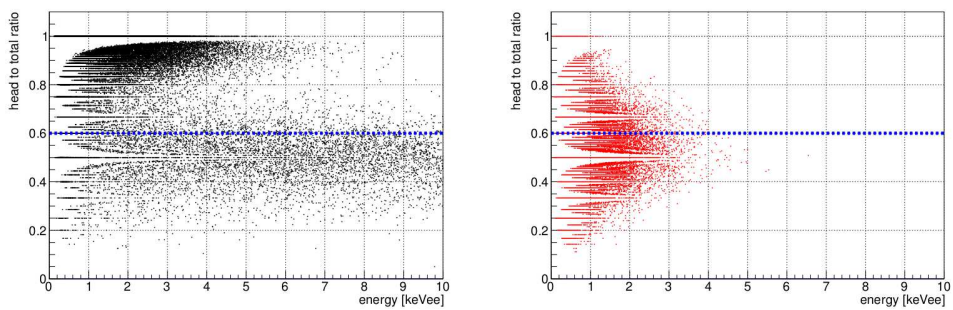


Figure 4: The Cherenkov event (head-to-total ratio  $> 0.6$ ) cut for the XMASS data (left) and for simulated WIMP events (right) as a function of the observed energy.

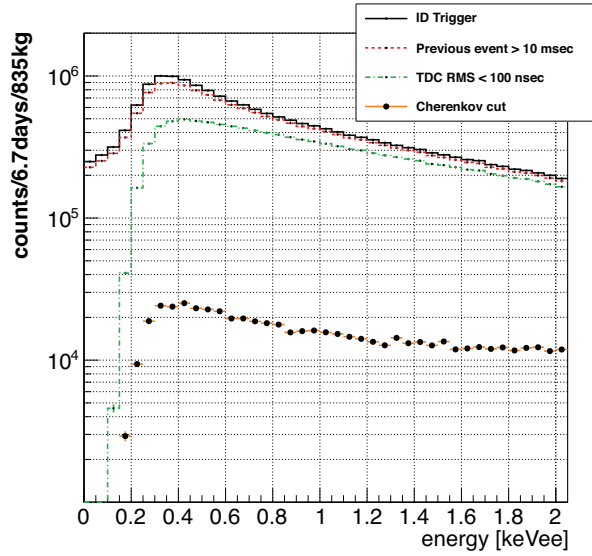


Figure 5: The obtained energy spectrum at each step of the data reduction. Raw data is shown as the solid line, the result of the 10 ms to the previous event timing cut appears as the dashed line, and the dash-dotted line shows the data after application of the timing distribution width cut. The filled points show the result of the Cherenkov event cut. Details are presented in the text.

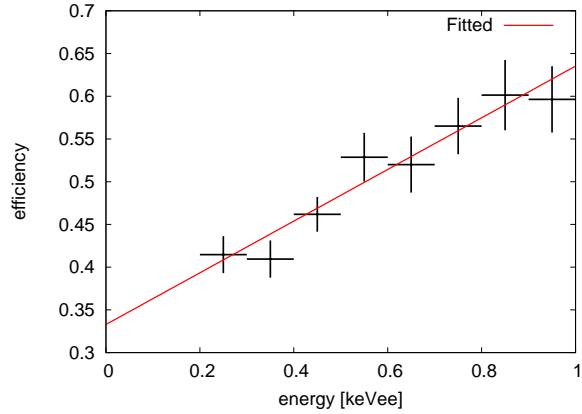


Figure 6: WIMP signal acceptance efficiency after data reduction for the analysis.

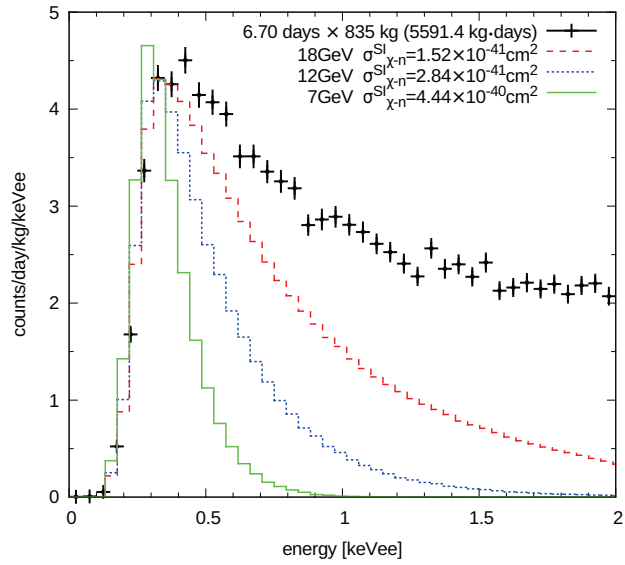


Figure 7: Simulated WIMP energy spectra in the XMASS detector assuming the maximum cross section that provides a signal rate no larger than the observation in any bin above 0.3 keVee.

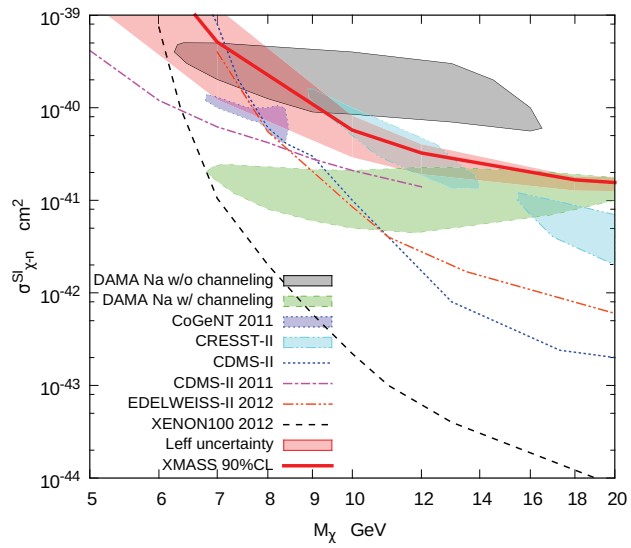


Figure 8: Spin-independent elastic WIMP-nucleon cross section as a function of WIMP mass. All systematic uncertainties except that from  $\mathcal{L}_{\text{eff}}$  are taken into account in the XMASS 90% C.L. limit line. The effect of the  $\mathcal{L}_{\text{eff}}$  uncertainty on the limit is shown in the band. Limits from other experiments and favored regions are also shown [4, 5, 6, 7, 8, 9].